Published as: *Cell*. 2015 September 24; 163(1): 123–133.

Phase separation by low complexity domains promotes stress granule assembly and drives pathological fibrillization

Amandine Molliex[1], **Jamshid Temirov**[2], **Jihun Lee**[3], **Maura Coughlin**[1], **Anderson P. Kanagaraj**[1], **Hong Joo Kim**[1], **Tanja Mittag**[3,‡], and **J. Paul Taylor**[4,‡]

[1]Department of Cell and Molecular Biology, St. Jude Children's Research Hospital, Memphis, TN 38120, USA

[2]Cell and Tissue Imaging Center, St. Jude Children's Research Hospital, Memphis, TN 38120, USA

[3]Department of Structural Biology, St. Jude Children's Research Hospital, Memphis, TN 38120, USA

[4]Howard Hughes Medical Institute, Department of Cell and Molecular Biology, St. Jude Children's Research Hospital, Memphis, TN 38120, USA

SUMMARY

Stress granules are membrane-less organelles composed of RNA-binding proteins (RBPs) and RNA. Functional impairment of stress granules has been implicated in amyotrophic lateral sclerosis, frontotemporal dementia and multisystem proteinopathy - diseases that are characterized by fibrillar inclusions of RBPs. Genetic evidence suggests a link between persistent stress granules and the accumulation of pathological inclusions. Here we demonstrate that the RBP hnRNPA1 undergoes liquid-liquid phase separation (LLPS) into protein-rich droplets mediated by a low complexity sequence domain (LCD). While the LCD of hnRNPA1 is sufficient to mediate LLPS, the RNA recognition motifs contribute to LLPS in the presence of RNA, giving rise to several mechanisms for regulating assembly. Importantly, while not required for LLPS, fibrillization is enhanced in protein-rich droplets. We suggest that LCD-mediated LLPS contributes to the assembly of stress granules and their liquid properties, and provides a mechanistic link between persistent stress granules and fibrillar protein pathology in disease.

Keywords

phase transition; liquid-liquid demixing; RNA-binding protein; ALS; RNA granules; amyloid

‡Correspondence: J. Paul Taylor, MD. Ph.D., jpaul.taylor@stjude.org or Tanja Mittag, Ph.D., tanja.mittag@stjude.org.

AUTHOR CONTRIBUTIONS

A.M., H.J.K., T.M. and J.P.T. designed experiments. A.M., J.T., J.L., M.C., A.P.K. H.J.K. and T.M. performed the experiments. A.M., J.T., H.J.K., T.M. and J.P.T. contributed to data analysis. A.M., H.J.K, T.M. and J.P.T. wrote the manuscript.

INTRODUCTION

It has recently emerged that cells organize many biochemical processes in membrane-less compartments that have liquid-like properties, exemplified by germ granules in *C. elegans* and nucleoli in *X. laevis* (Brangwynne et al., 2009; Brangwynne et al., 2011). It has been proposed that membrane-less organelles arise through a process of liquid-liquid phase separation (LLPS), which permits the requisite components of membrane-less organelles to become rapidly and reversibly concentrated in discrete loci in cells (Hyman et al., 2014). Although the molecular details underlying LLPS in cells are largely obscure, several recent reports indicate that constituent proteins harboring intrinsically disordered, low complexity sequence domains (LCDs) can mediate this process. For example, RNA helicase DDX4, a LCD-containing constituent of germ granules, forms phase-separated organelles that exhibit liquid properties *in vitro* and in live cells (Nott et al., 2015). Related, LAF-1 undergoes LLPS *in vitro* and is required for P granule assembly in *C. elegans* (Elbaum-Garfinkle et al., 2015). Additional RNA/protein assemblies similarly are membrane-less organelles that exhibit liquid properties and may assemble by LLPS, including stress granules, P bodies and Cajal bodies (Hyman et al., 2014; Wippich et al., 2013).

Stress granules are membrane-less cytosolic bodies composed of mRNAs and proteins that assemble when translation initiation is limiting, and are thought to represent a pool of mRNPs stalled in the process of translation initiation (Anderson and Kedersha, 2009; Buchan and Parker, 2009). A wealth of genetic evidence has emerged over the past 5 years implicating stress granules as a subcellular compartment that is central to the pathogenesis of a closely related set of degenerative diseases, including amyotrophic lateral sclerosis (ALS), frontotemporal dementia (FTD) and inclusion body myopathy (IBM) (Li et al., 2013; Ramaswami et al., 2013). These degenerative diseases are characterized pathologically by cytoplasmic inclusions composed of fibrillar deposits of heterogeneous nuclear ribonucleoproteins (hnRNPs) in affected cells (Kim et al., 2013; Ramaswami et al., 2013). Conspicuously, inherited forms of ALS, FTD and myopathy are often caused by missense mutations impacting hnRNPs, such as TDP-43, FUS, hnRNPA1, hnRNPA2B1, hnRNPDL and TIA-1 (Kim et al., 2013; Klar et al., 2013; Kwiatkowski et al., 2009; Sreedharan et al., 2008; Vieira et al., 2014). These hnRNPs are all components of stress granules and disease-causing mutations in these proteins are associated with accumulation of persistent stress granules (Bosco et al., 2010; Hackman et al., 2013; Kim et al., 2013). ALS, FTD and myopathy are also caused by mutations in VCP/p97, which are associated with impaired autophagic clearance of stress granules (Buchan et al., 2013). ALS-causing mutations in the actin-binding protein Profilin 1 similarly impair stress granule dynamics (Figley et al., 2014). Thus, a variety of genetic and cell biological insights have focused attention on alteration in stress granule dynamics as a key defect in the pathogenesis of ALS, FTD and myopathy, yet the mechanism that leads to accumulation of fibrillar hnRNP pathology remains obscure.

hnRNPA1 is a prototypical hnRNP consisting of two folded RNA recognition motifs (RRMs) that occupy the N-terminal half of the protein and a low complexity sequence domain (LCD) that occupies the C-terminal half. Missense mutations in the LCD of hnRNPA1 cause ALS and multisystem proteinopathy (MSP), a pleiotropic degenerative

disorder affecting muscle and brain (Bosco et al., 2010; Hackman et al., 2013; Kim et al., 2013). hnRNPA1 and closely related hnRNPs exhibit intrinsic propensity to assemble into amyloid-like fibrils containing cross-β-structure and this property has been proposed to mediate stress granule assembly (Kato et al., 2012). However, stress granules are dynamic assemblies; its components have residence times varying between seconds and minutes and, indeed, the assembly and disassembly of entire granules are accomplished on this same time scale (Buchan and Parker, 2009). These rapid dynamics argue in favor of a mechanism that permits rapid assembly and disassembly, such as LLPS, and suggest that rather than accounting for their assembly, fibrillization by hnRNPA1 and related hnRNPs may represent specialized components that accrue within stress granules. Here we demonstrate that the RBP hnRNPA1 undergoes LLPS mediated by the LCD to form protein-rich droplets. While the LCD of hnRNPA1 is sufficient to mediate phase separation, the folded RNA recognition motifs contribute to phase separation in the presence of RNA, giving rise to several mechanisms for regulating assembly. Importantly, while not required for phase separation, fibrillization is enhanced in protein-rich droplets. These results suggest that LCD-mediated LLPS contributes to the assembly of stress granules and their liquid properties, and reveals the mechanistic link between persistent stress granules and fibrillar protein pathology in disease.

RESULTS

hnRNPA1 undergoes liquid-liquid phase separation

To gain insight into the role of individual RBPs with LCDs in the assembly of stress granules, we expressed and purified hnRNPA1 and TDP-43 as fusions with solubility-enhancing His-SUMO tags (His-SUMO-hnRNPA1 and His-SUMO-TDP-43). Importantly, this purification always included careful RNA digestion followed by ion exchange and gel filtration chromatography to remove all nucleotides (Figure S1). The hnRNPA1 solution exhibited temperature-dependent reversible turbidity (Figure 1A), which was revealed by differential interference contrast microscopy to reflect the presence of numerous droplets (Figure 1B). The His-SUMO-TDP-43 solution was also turbid due to the presence of a multitude of small droplets (Figure 1C). The formation of hnRNPA1 droplets was inducible by a decrease in temperature, was rapidly reversible, and required a minimum protein concentration that was dependent on temperature (Movie S1). Droplets of hnRNPA1 exhibited wetting when they encountered the surface of the coverslip, suggesting liquid properties (Figure 1D and Movie S2). To further probe the nature of the droplets, we fluorescently labeled hnRNPA1 by conjugation to Oregon Green, and observed that these protein droplets tended to fuse rapidly into larger droplets within seconds, further reflecting liquid properties (Figure 1E, Movie S3). Removal of the His-SUMO tag from hnRNPA1 led to the same observations, demonstrating that properties intrinsic to hnRNPA1 mediate the ability for assembly into droplets (Figure S2). We assessed the mobility of hnRNPA1 molecules between the droplet and bulk phases by fluorescence recovery after photobleaching (FRAP) measurements (Figure 1F). After photobleaching a single droplet, the majority of its fluorescence signal (~80%) recovered with a characteristic recovery time of 3.7 s (Table S1). These data demonstrated that hnRNPA1 is highly dynamic, with rapid exchange of molecules between the droplets and the surrounding solution. The appearance

of this second liquid phase in a temperature- and protein concentration-dependent manner is consistent with LLPS by hnRNPA1 as described by Flory-Huggins theory (Flory, 1942; Huggins, 1942). hnRNPA1 is also able to assemble into hydrogels composed of uniformly polymerized amyloidlike fibers (Kato et al., 2012). We produced hydrogels from purified His-SUMO-hnRNPA1 according to the protocol of (Kato et al., 2012); thus, purified hnRNPA1 was dialyzed at 4 °C overnight, sonicated, concentrated and incubated for 48 hours at room temperature resulting in hydrogel formation. While hnRNPA1 hydrogels exhibit dynamic properties (Kato et al., 2012), they did not show any detectable fluorescence recovery after photobleaching in experiments lasting >15 minutes (Figure 1G and 1H), demonstrating that hnRNPA1 is more rigidly incorporated into hydrogels than into liquid droplets. These data are in agreement with the report that hnRNPA1 hydrogels are composed of cross-β fibrils, which may represent a thermodynamically stabilized or kinetically trapped state of the protein. While hnRNPA1 droplets showed a wide size distribution and grew over time by fusion events, TDP-43 droplets were similar in size with an upper limit of ~1 μm, and often appeared in strings as if fusion events into larger droplets were initiated but did not proceed (Movie S4). Their spherical nature suggested that they were also formed by LLPS, but since the material properties of TDP-43 droplets appeared more complex than classic liquid we focused on the underlying biophysical interactions of hnRNPA1 LLPS going forward.

LLPS has been proposed as the molecular mechanism underlying formation of membrane-less cellular bodies that exhibit liquid properties, such as P bodies and nucleoli (Brangwynne et al., 2009; Elbaum-Garfinkle et al., 2015; Fromm et al., 2014; Li et al., 2012; Nott et al., 2015). We observed that stress granules in cells exhibit liquid properties, regularly fusing into larger structures (Figure 1I; Movie S5). Moreover, hnRNPA1 in stress granules is in dynamic equilibrium with the surrounding cytosol, as illustrated by FRAP measurements showing similar recovery times (4.2 s) to purified hnRNPA1 in liquid droplets (Figure 1J). These classic liquid properties suggest that stress granules represent a separate liquid phase that is formed via LLPS.

The LCD of hnRNPA1 mediates liquid-liquid phase separation and is sufficient for incorporation into stress granules

In order to map the domains responsible for LLPS of hnRNPA1, we engineered His-SUMO fusion constructs containing either the folded N-terminal RNA recognition motifs (A1-RRM) or the C-terminal low complexity sequence domain (A1-LCD) (Table S2), which is predicted to be intrinsically disordered (Figure 2A; Figure S3). The A1-LCD alone had the ability to form liquid droplets, whereas A1-RRM failed to undergo LLPS under comparable conditions to full length hnRNPA1 (A1-FL) and all other conditions tested (Figure 2B). hnRNPA1 amino acid residues 259–264 correspond to a steric zipper motif centered in the LCD and are essential to hnRNPA1's intrinsic tendency to fibrillize (Kim et al., 2013). Importantly, the corresponding deletion mutant (A1-Δhexa), which does not fibrillize (Kim et al., 2013), readily undergoes LLPS, demonstrating that LLPS and fibrillization are two mechanistically distinct processes (Figure 2A and 2B). To test the role of LCD-mediated LLPS in the formation of stress granules, we transiently expressed wild-type, GFP-tagged LCD from hnRNPA1 (GFP-LCD) or a version with deletion of aa259–264 constituting the

steric zipper (GFP-LCD Δhexa) in HeLa cells (Figure 2C). Both of these proteins were efficiently incorporated into stress granules, suggesting that stress granule assembly does not require fibrillization and hence is distinct from hydrogel formation (Figure 2D and 2E).

Liquid-liquid phase separation by hnRNPA1 is based on weak interactions

To gain further insight into the intermolecular interactions underlying LLPS by hnRNPA1, we measured the temperature at which droplets first formed as a function of protein concentration and molecular crowding, allowing the construction of a phase diagram (Figure 3A). Whereas LLPS by hnRNPA1 occurs spontaneously in a temperature- and protein concentration-dependent manner in the absence of a crowding agent (Figure S4A), we mapped the phase diagram in the presence of Ficoll, a typical crowding agent, to mimic the crowded cellular environment, which is thought to contain ~200 mg/ml of macromolecules (Ellis, 2001). Ficoll was used for most experiments, but polyethylene glycol (PEG) was also able to promote hnRNPA1 LLPS (Figure S4B). These data demonstrated that the propensity for phase separation increased with increased molecular crowding, and the hnRNPA1 concentration necessary for phase separation drops substantially approaching conditions of intracellular molecular crowding. From the shape of the phase diagram, we conclude that hnRNPA1 has an upper critical solution temperature (UCST), *i.e.* a critical temperature exists, above which the two-phase regime cannot be accessed. A UCST phase diagram indicates that LLPS is driven mostly by enthalpy, with favorable interactions between protein molecules mediating assembly (Flory, 1942; Huggins, 1942). We also observed that lowering the NaCl concentration led to LLPS at lower A1-FL concentrations, suggesting that electrostatic interactions contributed to LLPS. Again, the hnRNPA1 concentration necessary for phase separation dropped substantially approaching conditions of intracellular salt concentration (Figure 3B). Interestingly, LLPS by A1-FL was disrupted by hexanediol, a compound that disables the selectivity filter of the nuclear pore complex by disrupting the interactions of phenylalanines in the FG repeats (Patel et al., 2007; Ribbeck and Gorlich, 2002), suggesting that aromatic residues in the LCD contribute to LLPS of hnRNPA1 (Figure 3C). These results indicate that multiple types of favorable molecular interactions contribute to hnRNPA1 LLPS.

Increasing the cytoplasmic concentration of endogenous LCD-containing hnRNPs is sufficient to drive stress granule assembly

To manipulate the cytoplasmic concentration of endogenous hnRNPA1 and related hnRNPs in cells we transiently expressed M9M peptide in HeLa cells. M9M peptide was designed to have a significantly greater affinity for Karyopherin-β2 than natural PY-NLSs present in hnRNPA1 and several closely related RNA-binding proteins (Bernis et al., 2014; Cansizoglu et al., 2007). As a result, M9M prevents Karyopherin-β2 from binding a select subset of PY-NLS-containing endogenous clients and results in their accumulation in the cytoplasm (Cansizoglu et al., 2007; Dormann et al., 2012). We observed that transient expression of YFP-M9M in HeLa cells resulted in increased cytoplasmic concentration of hnRNPA1 and related LCD-containing RNA-binding proteins (hnRNPA2 and FUS) resulting in an increased assembly of stress granules compared to the cells transfected with YFP only (Figure 3D–E, Figure S5A and S5B). Together with the *in vitro* data, these observations

suggest that concentration-dependent LLPS drives assembly of stress granules and requires a threshold protein concentration.

RNA facilitates liquid-liquid phase separation by hnRNPA1 by binding to RRMs and LCD

Stress granules are enriched in RNA-binding proteins and translationally-stalled mRNAs (Kedersha and Anderson, 2002). hnRNPA1 contains two RNA recognition motifs (Figure 2A) that have been shown to bind RNA (Burd and Dreyfuss, 1994), thus we tested whether the association with RNA plays a role in hnRNPA1 phase separation properties. Based on CLIP-seq, hnRNPA1 has been shown to bind >1000 RNA species through a relatively short, degenerate sequence motif (Huelga et al. Cell Rep. 2012). Thus, rather than engineer a specific sequence we used a random oligonucleotide RNA sequence. Fluorescently-labeled RNA (fl-RNA^{44}) was recruited into the protein-dense droplets formed by hnRNPA1 (Figure 4A). Notably, the addition of RNA substantially decreased the hnRNPA1 concentration required for phase separation to as low as 500 nM, well within the estimated intracellular concentration of hnRNPA1 (Figure 4B and Supplemental Information). The increased propensity for LLPS in the presence of RNA suggested the formation of larger hetero-oligomers. Indeed, despite our previous results that A1-RRM alone was not able to undergo LLPS under any conditions when tested in isolation, it readily phase separated in the presence of RNA. The two RRM domains and multiple binding motifs for RRMs on the RNA likely mediate weak multivalent interactions that lead to LLPS. Droplets formed by A1-LCD also recruited RNA, indicating that the LCD of hnRNPA1 binds RNA, as shown previously (Mayeda et al., 1994). Indeed, using fluorescence anisotropy, we confirmed that A1-FL, A1-RRM and A1-LCD interacted with fl-RNA^{44} with low micromolar affinity (Figure 4D). In this experiment, we added increasing concentrations of the indicated proteins to fl-RNA^{44}. Protein binding to RNA slows the tumbling of this labeled species and this is detected by an increase in fluorescence anisotropy and the inflection point on the curve corresponds approximately to the dissociation constant of the interaction. Thus, RNA can bind the RRM domains as well as the LCD in hnRNPA1 and this multivalency likely results in the formation of large higher-order complexes that promote LLPS of hnRNPA1 more efficiently than via the LCD alone. Our findings suggest a mechanism by which multivalent interactions between RNA and some RNA-binding proteins may contribute to the formation of stress granules.

Disease-causing mutation to hnRNPA1 does not significantly alter liquid-liquid phase separation properties

The disease-causing hnRNPA1 mutant, D262V, was associated with increased stress granule assembly as well as formation of hnRNPA1 fibrils, but the relationship of these observations was unclear (Kim et al., 2013). To examine the impact of disease mutation on LLPS of hnRNPA1, we expressed and purified His-SUMO-hnRNPA1-D262V (A1-D262V) and determined that this mutant protein undergoes spontaneous temperature- and concentration dependent LLPS to create liquid droplets that were morphologically indistinguishable from liquid droplets formed by wild-type protein (Movie S6). Assessment of A1-D262V in liquid droplets by FRAP showed a recovery time of similar duration (2.9 s) to that of wild-type hnRNPA1 illustrating that the mutation did not significantly impact dynamic exchange with the surrounding solution – at least in the time frames examined (Figure 5A). We mapped the

phase diagram of mutant hnRNPA1 in the presence of molecular crowder (Ficoll at 100 mg/ml) and 300 mM NaCl and found no significant differences from that of wild-type hnRNPA1 (Figure 5B). Finally, we observed that wild-type and mutant hnRNPA1 were miscible in droplets (Figure 5C). Together these results suggest that the disease-causing mutation does not significantly impact the interactions that drive phase separation.

Liquid-liquid phase separation promotes fibrillization of the disease-causing mutant

While examining the LLPS properties of A1-D262V we noted that reversible droplet assembly was accompanied by the accumulation of insoluble precipitate on the coverslip surface (Figure 6A). After the temperature was raised and the droplets dispersed, the surface of the coverslip was found to be blanketed with Thioflavin-T (ThT) positive fibrils (Figure S6). This phenomenon occurred within minutes of droplet assembly by A1-D262V and was not observed with wild-type hnRNPA1 or A1-Δhexa. We tested the fibrillization propensity of the His-SUMO tagged proteins under agitation at 25 °C by ThT fluorescence and observed substantially greater fibrillization of the mutant compared to wild-type, while hnRNPA1-Δhexadid not fibrillize over a period of 24 hours (Figure 6B). Fibrillization by A1-D262V under these conditions occurred on a time scale of hours, consistent with previous results (Kim et al., 2013). To observe the effect of LLPS on fibrillization, we mixed purified wild-type hnRNPA1 and mutant hnRNPA1 under conditions that allowed LLPS and noted that fibrils of mutant hnRNPA1 formed almost immediately in the floating condensed liquid droplets (Figure 6C) and gradually deposited on the coverslip surface (Figure 6D). Interestingly, we observed that mutant hnRNPA1 fibrils eventually seeded the assembly of wild-type hnRNPA1 resulting in mixed fibrils on the coverslip surface (Figure 6D), consistent with the previous observation that preformed fibrils of hnRNPA1 can seed assembly (Kim et al., 2013). To further illustrate the role of phase separation in driving fibrillization, we investigated the temporal correlation of the onset of fibrillization with LLPS. The protein was held in the one-phase regime (33 °C) or held in the two-phase regime (16 °C) by decreasing the temperature at different time points (0 min and 20 min). Mutant hnRNPA1 always formed fibrils immediately upon LLPS at either early or late time points, but never formed fibrils when the protein was maintained in the one-phase regime over the same period of time (Figure 6E). Taken together our findings demonstrate that LLPS increases the propensity of hnRPA1-D262V to form amyloid-like fibrils, likely by increasing the local protein concentration in droplets and enhancing nucleation. The presence of wild-type protein in droplets, or presumably other RBPs at risk for aggregation in stress granules, such as TDP-43, leads to its co-recruitment into fibrils.

DISCUSSION

We showed that the RBPs hnRNPA1 and TDP-43, disease proteins that are typical components of stress granules, are able to assemble into protein-rich droplets via LLPS (Figure 1). The LCD of hnRNPA1 mediates LLPS *in vitro* and is sufficient for recruitment into stress granules in cells (Figure 2). LLPS of hnRNPA1 is tunable by environmental conditions; specifically, lower salt concentration, molecular crowding, and interaction with RNA all reduce the protein concentration required for LLPS to a physiologically relevant range (Figures 3 and 4). Forced increase in the cytoplasmic concentration of hnRNPA1 and

closely related RBPs is sufficient to drive stress granule assembly, consistent with an LLPS-mediated process (Figure 3). Fibrillization of hnRNPA1 promoted by a potent steric zipper in the LCD is dispensable for LLPS and for the recruitment of the LCD to stress granules (Figure 2). Furthermore, protein molecules can exchange between the protein-poor and protein–rich phases on a time scale of seconds, consistent with the dynamics observed in stress granules in cells (Figure 1). By contrast, LCD-containing RBPs are more rigidly incorporated into hydrogels composed of uniformly polymerized amyloid-like fibers ((Kato et al., 2012) and Figure 1). Nevertheless, it is evident that a propensity toward fibrillization is a conserved feature of LCD-containing RBPs, possibly due to the sequence features giving rise to LLPS and specific interactions with other binding partners. The fibrillization propensity may also be physiologically relevant to stress granule function as has been previously suggested (Kato et al., 2012), perhaps representing a process of maturation after assembly is initiated by LLPS. On the other hand, the propensity toward fibrillization within the condensed liquid environment of stress granules also poses a risk, particularly when the LCD contains a fibril-promoting mutation (such as the disease-causing D262V mutation in hnRNPA1), which can lead to excess, pathological fibrillization as observed in ALS, FTD, myopathy and MSP, and as predicted by Weber and Brangwynne (Weber and Brangwynne, 2012) (Figures 6 and 7).

LCD sequence properties promoting LLPS

Proteins harboring LCDs are abundant in RNA granules and other membrane-less organelles (Anderson and Kedersha, 2006; Buchan and Parker, 2009; Voronina et al., 2011). Our finding that the LCD of hnRNPA1 mediates LLPS is consistent with recent reports that LCD-mediated LLPS of the DEAD-box helicases Ddx4 and Laf-1 play roles in the assembly of P granules (Elbaum-Garfinkle et al., 2015; Nott et al., 2015). As with generic IDPs (Das and Pappu, 2013; Das et al., 2015; Muller-Spath et al., 2010), amino acid composition and sequence patterning likely determine interactions within and conformational properties of LCDs and encode their ability to undergo phase separation. What might these features be? We find that LLPS of hnRNPA1 is enthalpy driven, and that aromatic and electrostatic interactions are driving forces (Figure 3). Indeed, hnRNPA1 is enriched in the aromatic residues phenylalanine and tyrosine, and the positively charged residue arginine relative to the overall eukaryotic proteome (Hormoz, 2013). Moreover, the LCD sequence of hnRNPA1 is patterned; phenylalanine and tyrosine residues are relatively evenly distributed with a mean spacing of 6.2 ± 2.3 residues (Figure S7). Positively charged residues, mainly arginines, are also well distributed (Figure S7). They may thus represent reiterated interaction motifs in the background of a polar polymer and enable multivalent interactions that drive LLPS.

Multivalent RNA/RRM domains mediate assembly of large complexes

Stress granules are, of course, composed not only of RBPs, but also untranslated mRNAs (Buchan and Parker, 2009; Teixeira et al., 2005), posing the question what role RNA plays in mediating LLPS of RBPs. Upon LLPS of a mixture of hnRNPA1 and RNA, we find that RNA not only localizes to the dense protein phase but reduces the hnRNPA1 concentrations required for LLPS. RNA likely engages hnRNPA1 in a multivalent fashion via both the RRM domains and the LCD, resulting in large, cross-linked complexes that undergo LLPS

at reduced concentrations. This interpretation is supported by several findings: (1) the folded RRM domains alone do not phase separate in the absence of RNA under any conditions tested, (2) RNA promotes LLPS of the RRM domains, presumably by engaging the two RRM domains in a multivalent fashion via several nucleotide motifs as was previously shown for PTB/RNA interactions (Li et al., 2012) resulting in large, cross-linked complexes and (3) the LCD also binds RNA. Thus, our results suggest that both protein-protein and protein-RNA interactions work synergistically in the assembly of RNA granules.

Fibrillization of RBPs in stress granules – pathology or physiological function?

hnRNPA1 is intrinsically prone to fibrillization - a propensity that is strongly enhanced by mutations that cause ALS and MSP (Kim et al., 2013). While fibrillization is not required for LLPS, and disease mutation does not significantly impact LLPS behavior on short time scales (Figure 5), fibrillization of mutant hnRNPA1 is enhanced in the two-phase regime (Figure 6). We propose that the high local protein concentration in the condensed liquid droplets increases the probability of rare nucleation events and of the rate constant for adding monomers to a growing fibril, in agreement with typical nucleation-driven fibrillization processes (Eisenberg and Jucker, 2012). Changes in the conformational ensemble and dynamics of the LCD compared to the dispersed state may also play roles in enhanced nucleation (Pappu et al., 2008). Nevertheless, the fact that wild type hnRNPA1 is prone to fibrillization on longer time scales, a behavior shared by a large number of related RBPs (Zhu et al., 2012) suggests that this property could occur in the context of RNA granules in cells and potentially contribute to physiological functions. For example, the formation of short length-scale dynamic fibrils might assemble in the condensed liquid phase during maturation of long-lived RNA granules and play functional roles or provide mechanical stability.

Irrespective of a potential physiological role in normal stress granules, our findings provide a model to explain the relationship between disease-associated genetic mutations that promote stress granule formation or prolong their assembly (Figure 7), and the fibrillar pathology that dominates end-stage disease. Thus we propose that the condensed liquid state of stress granules resulting from LLPS of hnRNPA1 and related RBPs, presents a very low probability risk of assembling amyloid-like fibrils that under normal conditions can be managed by granule disassembly and cellular proteostasis machinery. However, when stress granules are composed of RBPs that contain LCD mutations that promote fibrillization (Kim et al., 2013; Klar et al., 2013; Kwiatkowski et al., 2009; Sreedharan et al., 2008; Vieira et al., 2014), or when stress granules persist due to disturbances in disassembly machinery (Buchan et al., 2013; Figley et al., 2014), pathogenic fibrils can assemble and escape quality control surveillance.

EXPERIMENTAL PROCEDURES

Protein expression and purification

A1-FL, A1-RRM, A1-LCD, A1-D262V and A1-Δhexa were expressed as His-SUMO-tagged fusion proteins in BL21-Gold (DE3) cells (Agilent) in LB medium. Cells were lyzed in 50 mM HEPES pH 7.5, 250 mM NaCl, 30 mM imidazole, 2 mM βME, 100 μg/ml RNAse

and Complete protease inhibitor cocktail (Roche) with a microfluidizer. The cleared lysate was loaded onto a gravity NiNTA column, washed with lysis buffer and eluted in 50 mM HEPES pH 7.5, 150 mM NaCl, 300 mM imidazole, 2 mM βME. The proteins were treated with 0.2 mg/ml RNase A (Roche) for 5 minutes at 37 °C. The proteins were purified by ion exchange chromatography with a HiTrap SP or Q column (GE Healthcare). The fractions were analyzed by SDS-PAGE gel, pooled and concentrated. They were then subjected to size exclusion chromatography on a Superdex 200 16/60 column (GE Healthcare) equilibrated in sample buffer, 50 mM HEPES pH 7.5, 300 mM NaCl and 5 mM DTT. The fractions were analyzed by SDS-PAGE gel, pooled, concentrated and stored at −80 °C. Dynamic light scattering was used to ensure that the proteins were monomeric. The RNA levels were analyzed by gel (Figure S1). hnRNPA1 WT was fluorescently labeled with Oregon green 488, hnRNPA1 D262V with Rhodamine Red-X (for details see Supplemental Experimental Procedures).

Formation of hnRNPA1 hydrogels

Purified A1-FL was dialyzed against a gelation buffer containing 50 mM Tris-HCl (pH 7.5), 150 mM NaCl, 1 mM TCEP, 0.1 mM EDTA and 1 mM benzamidine overnight at 4 °C. The protein solution was sonicated 10 s at a 13% power level on a Misonix ultrasonic liquid processor Model S4000. The protein solutions were concentrated to roughly 35 mg/ml. After centrifugation, a 0.5 μl droplet of the supernatant was deposited onto a glass-bottomed microscope dish (MatTek). The dish was sealed with parafilm and incubated for 2 days at RT. The method was adapted from a previous report (Kato et al., 2012).

Cell culture and transfection

HeLa and U2OS G3BP-GFP cells were cultured in DMEM (Hyclone) supplemented with 10% FBS (Hyclone) and GlutaMax-1X (GIBCO). The U2OS G3BP-GFP stable line was a gift from Paul Anderson. Cells were transfected using FuGENE6 transfection reagent (Roche), according to the manufacturer’s instructions.

FRAP methods and analysis

FRAP experiments were performed using a Marianas spinning disk confocal (SDC) imaging system on a Zeiss Axio Observer inverted microscope platform. Time lapse images of the sample were collected with 100 ms exposure time for 1 to 2 minutes at 5.6 frames per second using a Zeiss Plan-Apochromat 63× 1.4 NA oil objective and Evolve 512 EMCCD camera (Photometrics). Images were analyzed with SlideBook 6 software (3i). For FRAP analysis, mean fluorescence intensities from three regions of interests (ROIs) of time lapse images were computed. ROI-1 was the photobleached region/droplet, ROI-2 was drawn in the area/droplet not connected to the photobleached droplet and was used to correct for overall photobleaching due to imaging laser illumination. ROI-3 was defined as background and its signal was subtracted from both ROI-1 and ROI-2 signals. Such background and photobleaching corrected fluorescence intensity vs. time graphs were expressed in fractional form normalized by the pre-photobleach intensity (Axelrod et al., 1976). See also Table S1.

Immunofluorescence studies

Cells were fixed in 4% paraformaldehyde in phosphate-buffered saline (PBS), permeabilized with 0.5% Triton X-100 in PBS for 10 min, blocked with 5% goat serum in PBS for 45 min, and incubated with primary antibody for 1.5 h at RT. Primary antibodies were visualized with secondary antibodies conjugated with Alexa Fluor 488, Alexa Fluor 555 and Alexa Fluor 647 (Molecular Probes, Invitrogen), and nuclei were detected using DAPI. Stained cells were examined using a Zeiss LSM 780 NLO confocal microscope with Zeiss ZEN software.

In vitro determination of phase diagram

Samples were prepared by mixing the determined amount of protein, buffer and Ficoll PM 400 (Sigma). Apparent cloud points were measured using a Linkam PE100 thermal stage mounted on a Zeiss LSM 780 NLO microscope. Sealed sample chambers containing protein solutions comprised coverslips sandwiching two layers of 3M 300 LSE high temperature double sided tape (0.34 mm) and were taped on the PE100 silver heating/cooling block. The variance in the solution conditions was monitored with temperature. For each given hnRNPA1 concentration, the sample was equilibrated at 33 °C (one-phase regime). The temperature was then decreased at a rate of 2 °C/min until the initial appearance of droplets at the apparent cloud point. Each set of cloud points (three independent replicates) was fitted to the scaling relation for binary demixing from renormalization-group theory (Muschol and Rosenberger, 1997; Sengers, 1980; Stanley, 1971):

$$T = \mathrm{Tc}\left\{1 - A\left|\frac{\mathrm{Cc} - \mathrm{Cp}}{\mathrm{Cc}}\right|^{1/\beta}\right\}, \text{with a critical exponent} \beta = 0.325$$

Fluorescence anisotropy

An N-terminally fluorescently labeled RNA fl-RNA[44] with sequence GGGCCCCCGGGUACCGAGCUGCUAAUCAAAACAAAACAAAAGCU was purchased from Sigma. For direct FA binding assays, increasing concentrations of A1-FL, A1-RRM and A1-LCD were titrated into 40 nM fl-RNA[44] in a buffer containing 50 mM HEPES pH 7.5, 300 mM NaCl, 0.01% Triton and 5 mM DTT, and the FA monitored with a CLARIOstar plate reader (BMG Labtech) at 25 °C. We performed a standard fluorescence anisotropy binding experiment, in which we added increasing concentrations of the indicated proteins to fluorescein-labeled RNA. Protein binding to RNA slows the tumbling of this labeled species and this is detected by an increase in fluorescence anisotropy. Analysis was performed as described previously (Roehrl et al., 2004).

In vitro fibril formation assay with Thioflavin-T measurements

The experiment was performed as described previously (Kim et al., 2013). In brief, 100 μM A1-WT, A1-D262V and A1-Δhexa, respectively, were incubated at 25 °C under agitation for 24 h. Aliquots were removed at 0 and 24 h, added to a solution of 50 μM ThT and the fluorescence intensity at a wavelength of 450–550 nm determined.

Supplementary Material

Refer to Web version on PubMed Central for supplementary material.

Acknowledgments

We thank J. Peng for his help in estimating the intracellular hnRNPA1 concentrations. We thank V. Frohlich and the St. Jude Cell and Tissue Imaging Shared Resource for extended access to their microscopes. We thank M. Rosen and R. Parker for comments on our manuscript and for sharing data prior to publication. We thank M. Marzahn for scientific input and E. Enemark for sharing reagents. We thank J. Parobek and A-M. Hedges in St. Jude Biomedical Communications for photography of the test tubes. This work was supported by funding from the Muscular Dystrophy Association, the Packard Center for ALS Research, Target ALS and ALSAC.

REFERENCES

Anderson P, Kedersha N. RNA granules. J Cell Biol. 2006; 172:803–808. [PubMed: 16520386]

Anderson P, Kedersha N. Stress granules. Curr Biol. 2009; 19:R397–R398. [PubMed: 19467203]

Axelrod D, Koppel DE, Schlessinger J, Elson E, Webb WW. Mobility measurement by analysis of fluorescence photobleaching recovery kinetics. Biophys J. 1976; 16:1055–1069. [PubMed: 786399]

Bernis C, Swift-Taylor B, Nord M, Carmona S, Chook YM, Forbes DJ. Transportin acts to regulate mitotic assembly events by target binding rather than Ran sequestration. Mol Biol Cell. 2014; 25:992–1009. [PubMed: 24478460]

Bosco DA, Lemay N, Ko HK, Zhou H, Burke C, Kwiatkowski TJ Jr, Sapp P, McKenna-Yasek D, Brown RH Jr, Hayward LJ. Mutant FUS proteins that cause amyotrophic lateral sclerosis incorporate into stress granules. Hum Mol Genet. 2010; 19:4160–4175. [PubMed: 20699327]

Brangwynne CP, Eckmann CR, Courson DS, Rybarska A, Hoege C, Gharakhani J, Julicher F, Hyman AA. Germline P granules are liquid droplets that localize by controlled dissolution/condensation. Science. 2009; 324:1729–1732. [PubMed: 19460965]

Brangwynne CP, Mitchison TJ, Hyman AA. Active liquid-like behavior of nucleoli determines their size and shape in Xenopus laevis oocytes. Proc Natl Acad Sci U S A. 2011; 108:4334–4339. [PubMed: 21368180]

Buchan JR, Kolaitis RM, Taylor JP, Parker R. Eukaryotic stress granules are cleared by autophagy and Cdc48/VCP function. Cell. 2013; 153:1461–1474. [PubMed: 23791177]

Buchan JR, Parker R. Eukaryotic stress granules: the ins and outs of translation. Mol Cell. 2009; 36:932–941. [PubMed: 20064460]

Burd CG, Dreyfuss G. RNA binding specificity of hnRNP A1: significance of hnRNP A1 high-affinity binding sites in pre-mRNA splicing. EMBO J. 1994; 13:1197–1204. [PubMed: 7510636]

Cansizoglu AE, Lee BJ, Zhang ZC, Fontoura BM, Chook YM. Structure-based design of a pathway-specific nuclear import inhibitor. Nat Struct Mol Biol. 2007; 14:452–454. [PubMed: 17435768]

Das RK, Pappu RV. Conformations of intrinsically disordered proteins are influenced by linear sequence distributions of oppositely charged residues. Proc Natl Acad Sci U S A. 2013; 110:13392–13397. [PubMed: 23901099]

Das RK, Ruff KM, Pappu RV. Relating sequence encoded information to form and function of intrinsically disordered proteins. Curr Opin Struct Biol. 2015; 32:102–112. [PubMed: 25863585]

Dormann D, Madl T, Valori CF, Bentmann E, Tahirovic S, Abou-Ajram C, Kremmer E, Ansorge O, Mackenzie IR, Neumann M, et al. Arginine methylation next to the PY-NLS modulates Transportin binding and nuclear import of FUS. EMBO J. 2012; 31:4258–4275. [PubMed: 22968170]

Eisenberg D, Jucker M. The amyloid state of proteins in human diseases. Cell. 2012; 148:1188–1203. [PubMed: 22424229]

Elbaum-Garfinkle S, Kim Y, Szczepaniak K, Chen CC, Eckmann CR, Myong S, Brangwynne CP. The disordered P granule protein LAF-1 drives phase separation into droplets with tunable viscosity and dynamics. Proc Natl Acad Sci U S A. 2015

Ellis RJ. Macromolecular crowding: an important but neglected aspect of the intracellular environment. Curr Opin Struct Biol. 2001; 11:114–119. [PubMed: 11179900]

Figley MD, Bieri G, Kolaitis RM, Taylor JP, Gitler AD. Profilin 1 associates with stress granules and ALS-linked mutations alter stress granule dynamics. J Neurosci. 2014; 34:8083–8097. [PubMed: 24920614]

Flory PJ. Thermodynamics of High Polymer Solutions. The Journal of Chemical Physics. 1942; 10:51.

Fromm SA, Kamenz J, Noldeke ER, Neu A, Zocher G, Sprangers R. In vitro reconstitution of a cellular phase-transition process that involves the mRNA decapping machinery. Angew Chem Int Ed Engl. 2014; 53:7354–7359. [PubMed: 24862735]

Hackman P, Sarparanta J, Lehtinen S, Vihola A, Evila A, Jonson PH, Luque H, Kere J, Screen M, Chinnery PF, et al. Welander distal myopathy is caused by a mutation in the RNA-binding protein TIA1. Ann Neurol. 2013; 73:500–509. [PubMed: 23401021]

Hormoz S. Amino acid composition of proteins reduces deleterious impact of mutations. Sci Rep. 2013; 3:2919. [PubMed: 24108121]

Huggins ML. Some Properties of Solutions of Long-chain Compounds. The Journal of Physical Chemistry. 1942; 46:151–158.

Hyman AA, Weber CA, Julicher F. Liquid-liquid phase separation in biology. Annu Rev Cell Dev Biol. 2014; 30:39–58. [PubMed: 25288112]

Kato M, Han TW, Xie S, Shi K, Du X, Wu LC, Mirzaei H, Goldsmith EJ, Longgood J, Pei J, et al. Cell-free formation of RNA granules: low complexity sequence domains form dynamic fibers within hydrogels. Cell. 2012; 149:753–767. [PubMed: 22579281]

Kedersha N, Anderson P. Stress granules: sites of mRNA triage that regulate mRNA stability and translatability. Biochem Soc Trans. 2002; 30:963–969. [PubMed: 12440955]

Kim HJ, Kim NC, Wang YD, Scarborough EA, Moore J, Diaz Z, MacLea KS, Freibaum B, Li S, Molliex A, et al. Mutations in prion-like domains in hnRNPA2B1 and hnRNPA1 cause multisystem proteinopathy and ALS. Nature. 2013; 495:467–473. [PubMed: 23455423]

Klar J, Sobol M, Melberg A, Mabert K, Ameur A, Johansson AC, Feuk L, Entesarian M, Orlen H, Casar-Borota O, et al. Welander distal myopathy caused by an ancient founder mutation in TIA1 associated with perturbed splicing. Hum Mutat. 2013; 34:572–577. [PubMed: 23348830]

Kwiatkowski TJ Jr, Bosco DA, Leclerc AL, Tamrazian E, Vanderburg CR, Russ C, Davis A, Gilchrist J, Kasarskis EJ, Munsat T, et al. Mutations in the FUS/TLS gene on chromosome 16 cause familial amyotrophic lateral sclerosis. Science. 2009; 323:1205–1208. [PubMed: 19251627]

Li P, Banjade S, Cheng HC, Kim S, Chen B, Guo L, Llaguno M, Hollingsworth JV, King DS, Banani SF, et al. Phase transitions in the assembly of multivalent signalling proteins. Nature. 2012; 483:336–340. [PubMed: 22398450]

Li YR, King OD, Shorter J, Gitler AD. Stress granules as crucibles of ALS pathogenesis. J Cell Biol. 2013; 201:361–372. [PubMed: 23629963]

Mayeda A, Munroe SH, Caceres JF, Krainer AR. Function of conserved domains of hnRNP A1 and other hnRNP A/B proteins. EMBO J. 1994; 13:5483–5495. [PubMed: 7957114]

Muller-Spath S, Soranno A, Hirschfeld V, Hofmann H, Ruegger S, Reymond L, Nettels D, Schuler B. From the Cover: Charge interactions can dominate the dimensions of intrinsically disordered proteins. Proc Natl Acad Sci U S A. 2010; 107:14609–14614. [PubMed: 20639465]

Muschol M, Rosenberger F. Liquid-liquid phase separation in supersaturated lysozyme solutions and associated precipitate formation/crystallization. J Chem Phys. 1997; 107:1953–1962.

Nott TJ, Petsalaki E, Farber P, Jervis D, Fussner E, Plochowietz A, Craggs TD, Bazett-Jones DP, Pawson T, Forman-Kay JD, et al. Phase transition of a disordered nuage protein generates environmentally responsive membraneless organelles. Mol Cell. 2015; 57:936–947. [PubMed: 25747659]

Pappu RV, Wang X, Vitalis A, Crick SL. A polymer physics perspective on driving forces and mechanisms for protein aggregation. Arch Biochem Biophys. 2008; 469:132–141. [PubMed: 17931593]

Patel SS, Belmont BJ, Sante JM, Rexach MF. Natively unfolded nucleoporins gate protein diffusion across the nuclear pore complex. Cell. 2007; 129:83–96. [PubMed: 17418788]

Ramaswami M, Taylor JP, Parker R. Altered ribostasis: RNA-protein granules in degenerative disorders. Cell. 2013; 154:727–736. [PubMed: 23953108]

Ribbeck K, Gorlich D. The permeability barrier of nuclear pore complexes appears to operate via hydrophobic exclusion. EMBO J. 2002; 21:2664–2671. [PubMed: 12032079]

Roehrl MH, Wang JY, Wagner G. A general framework for development and data analysis of competitive high-throughput screens for small-molecule inhibitors of protein-protein interactions by fluorescence polarization. Biochemistry. 2004; 43:16056–16066. [PubMed: 15610000]

Sengers, JV. Universality of Critical Phenomena in Classical Fluids. In: Levy, JCLGaJZ-JM., editor. Phase Transitions. New York: Plenum Press; 1980. p. 95

Sreedharan J, Blair IP, Tripathi VB, Hu X, Vance C, Rogelj B, Ackerley S, Durnall JC, Williams KL, Buratti E, et al. TDP-43 mutations in familial and sporadic amyotrophic lateral sclerosis. Science. 2008; 319:1668–1672. [PubMed: 18309045]

Stanley, HE. Introduction to Phase Transitions and Critical Phenomena. New York: Oxford University Press; 1971.

Teixeira D, Sheth U, Valencia-Sanchez MA, Brengues M, Parker R. Processing bodies require RNA for assembly and contain nontranslating mRNAs. RNA. 2005; 11:371–382. [PubMed: 15703442]

Vieira NM, Naslavsky MS, Licinio L, Kok F, Schlesinger D, Vainzof M, Sanchez N, Kitajima JP, Gal L, Cavacana N, et al. A defect in the RNA-processing protein HNRPDL causes limb-girdle muscular dystrophy 1G (LGMD1G). Hum Mol Genet. 2014; 23:4103–4110. [PubMed: 24647604]

Voronina E, Seydoux G, Sassone-Corsi P, Nagamori I. RNA granules in germ cells. Cold Spring Harb Perspect Biol. 2011:3.

Weber SC, Brangwynne CP. Getting RNA and protein in phase. Cell. 2012; 149:1188–1191. [PubMed: 22682242]

Wippich F, Bodenmiller B, Trajkovska MG, Wanka S, Aebersold R, Pelkmans L. Dual specificity kinase DYRK3 couples stress granule condensation/dissolution to mTORC1 signaling. Cell. 2013; 152:791–805. [PubMed: 23415227]

Zhu Y, Liao S, Ye J, Zhang H. Cloning and characterization of a novel tyrosine ammonia lyase-encoding gene involved in bagremycins biosynthesis in Streptomyces sp. Biotechnol Lett. 2012; 34:269–274. [PubMed: 22065278]

HIGHLIGHTS

- hnRNPA1 undergoes spontaneous concentration-dependent liquid-liquid phase separation
- Liquid-liquid phase separation is mediated by a low complexity sequence domain
- Stress granules assemble in a RNA-binding protein concentration-dependent manner
- Pathological fibrillization of hnRNPA1 is driven by liquid-liquid phase separation

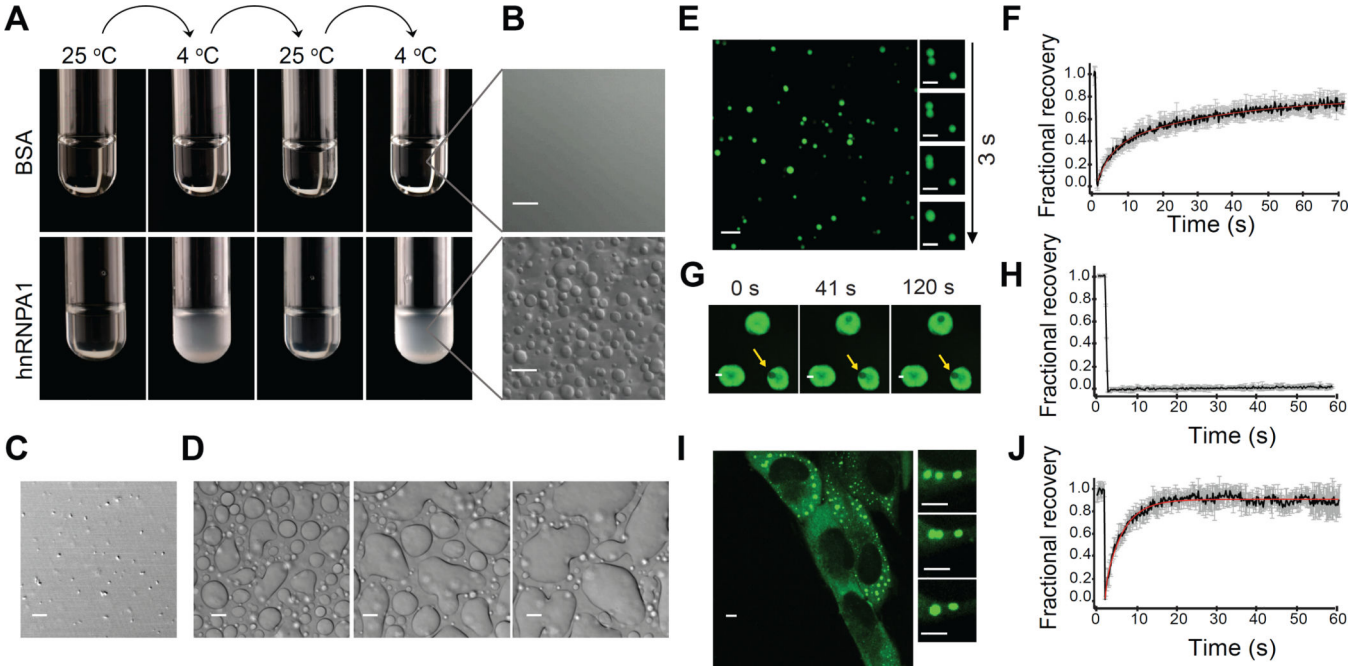

Figure 1. hnRNPA1 spontaneously and reversibly assembles into liquid droplets

(A) Test tubes containing 500 μM BSA or 500 μM His-SUMO-hnRNPA1, respectively, were alternated between 4 °C and 25 °C.

(B) Transparent BSA or turbid hnRNPA1 solution observed by differential interference contrast (DIC) microscopy at 10 °C.

(C) TDP-43 droplets observed by DIC at 25 °C.

(D) 300 μM hnRNPA1 in 100 mM NaCl exhibited wetting at the surface of the coverslip. Images were extracted from Movie S2.

(E) Fluorescence micrographs of hnRNPA1 (spiked with Oregon green-labeled hnRNPA1 at a molar ratio of 300:1) in 150 mM NaCl buffer at 10 °C reveal that the protein is enriched in the droplets; the droplets fuse over time. The main image and the panel on the right were extracted from Movie S3.

(F) FRAP of fluorescently labeled/unlabeled hnRNPA1 at a molar ratio of 1:300. The black curve is an average of FRAP events from 9 distinct droplets; the error bars represent the standard error. The red curve corresponds to a double exponential fit of the data. The two characteristic recovery times are 3.72 s and 31.6 s. See also Table S1.

(G) An area of hydrogel (white arrow) was photobleached over the course of 60 seconds. A decrease of the fluorescence intensity was observed, but no recovery. The yellow arrow points a piece of hydrogel photbleached 15 minutes before.

(H) FRAP of hydrogels. The black curve is an average of FRAP events from 3 different hydrogel pieces; the error bars represent the standard error.

(I) Live imaging of U2OS cells expressing G3BP-GFP. The cells were stressed for 1 h with 0.5 mM arsenite and stress granules formation was observed. Stress granules fused over time. The main image and the panel on the right were extracted from Movie S5.

(J) FRAP of hnRNPA1 in stress granules. The black curve is an average of FRAP events from 12 distinct stress granules from 12 distinct cells; the error bars represent the standard

error. The red curve corresponds to a single exponential fit of the data. The characteristic recovery time is 4.21 s. See also Table S1.

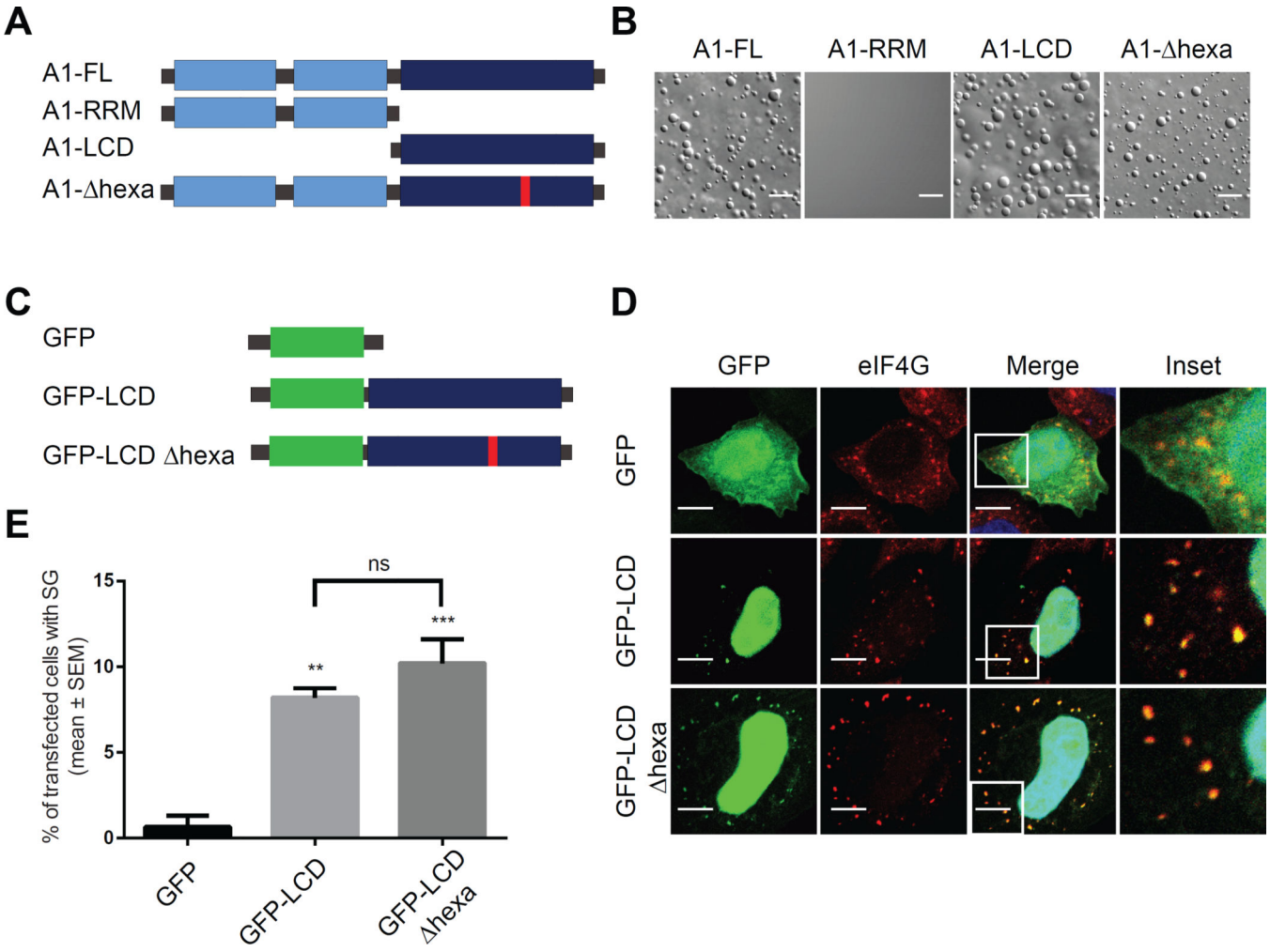

Figure 2. Liquid-liquid phase separation by hnRNPA1 is mediated by the C-terminal low complexity sequence domain and is distinct from fibrillization

(A) Schematic of the structure of hnRNPA1 full-length (A1-FL), of the N-terminus comprising the two folded RNA recognition motifs (A1-RRM), of the low complexity domain sequence (A1-LCD), and of the mutant with a deletion of residues 259–264 (Kim et al., 2013) (A1-Δhexa).

(B) DIC images of A1-FL, A1-RRM, A1-LCD and A1-Δhexa at 140 μM protein, 150 mg/ml Ficoll in 50 mM HEPES, 300 mM NaCl and 5 mM DTT.

(C) Schematic of the constructs transiently expressed in HeLa cells.

(D) Representative confocal microscopy images of HeLa cells transfected with constructs presented in (**C**), treated with 0.5 mM sodium arsenite for 15 min, and immunostained with anti-eIF4G (red) and DAPI (blue).

(E) Quantification for data in **(D)**. The percentage of transfected cells displaying GFP signal in SGs ((number of cells with GFP-positive SGs/number of GFP expressing cells) X 100) was plotted as mean ± s.e.m., n = 100 cells, ** $p < 0.005$, *** $p < 0.001$ by One Way ANOVA, Tukey's Post Hoc test.

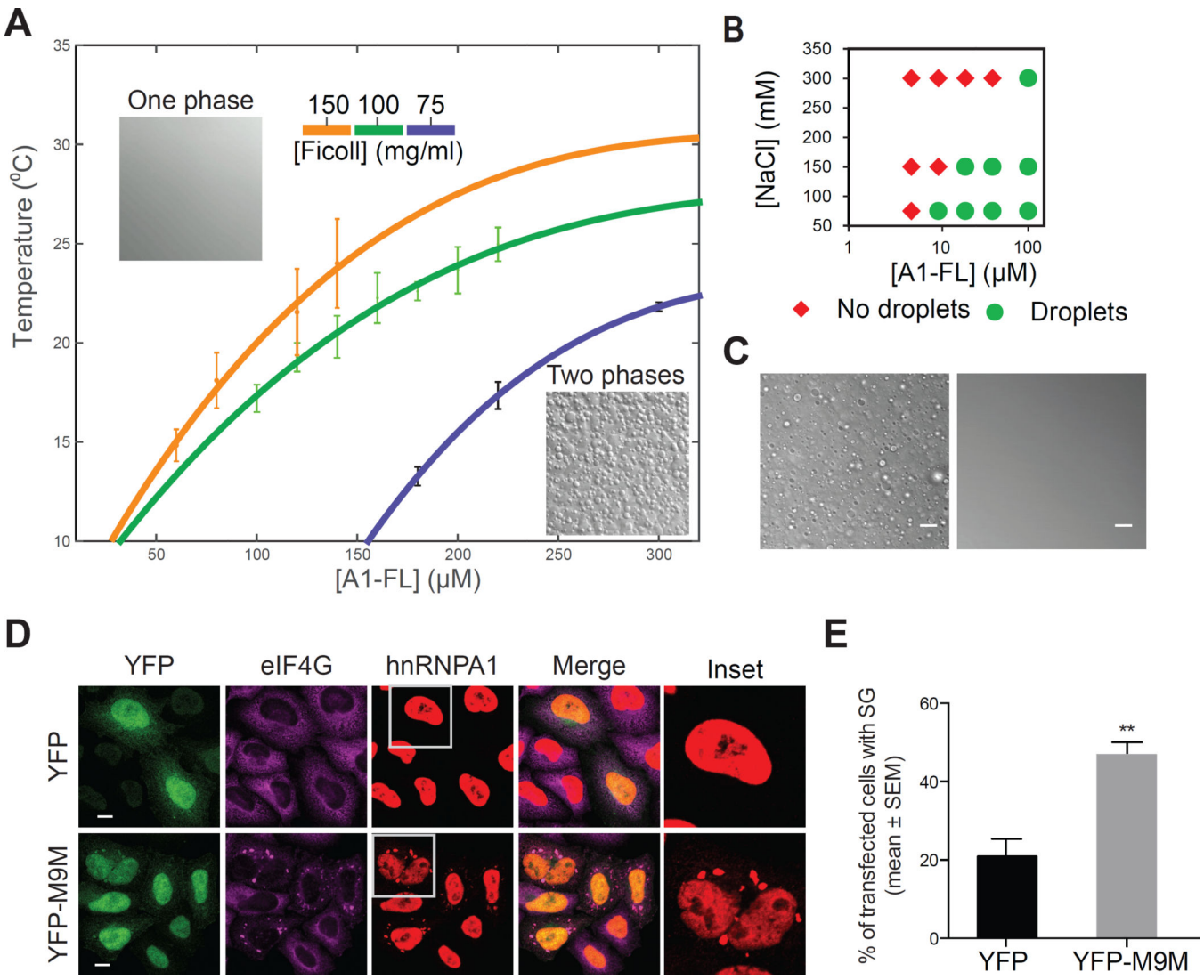

Figure 3. Molecular crowding, electrostatic and hydrophobic interactions and increased cytoplasmic concentration of hnRNPs contribute to liquid-liquid phase separation of hnRNPA1

(A) Phase diagrams of hnRNPA1 in 50 mM HEPES, 300 mM NaCl, 5 mM DTT. The apparent cloud point, i.e. the temperature at which droplets were first observed, was determined as a function of protein concentration and molecular crowding. Each point represents the mean of a triplicate ± SD. The solid curve represents a fit to a relation for binary demixing that describes the shape of the coexistence curve (Muschol and Rosenberger, 1997; Sengers, 1980; Stanley, 1971).

(B) Protein/NaCl concentration pairs scoring positive (green circles) or negative (red diamonds) for the appearance of droplets. The experiment was performed in 100 mg/ml Ficoll at 10 °C.

(C) DIC images of 100 μM hnRNPA1 and 150 mg/ml Ficoll at 10 °C; the solution returns to the one-phase regime upon the addition of 5% 1,6-hexanediol.

(D) Confocal microscopy images of HeLa cells transfected with YFP or YFP-M9M and immunostained with anti-hnRNPA1 (red) and anti-eIF4G (purple). The insets show hnRNPA1. See also Figure S5.

(E) Quantification for data in **(D)**. The percentage of transfected cells displaying SGs was plotted as mean ± s.e.m., n = 100 cells, ** $p < 0.005$ by One Way ANOVA, Tukey's Post Hoc test.

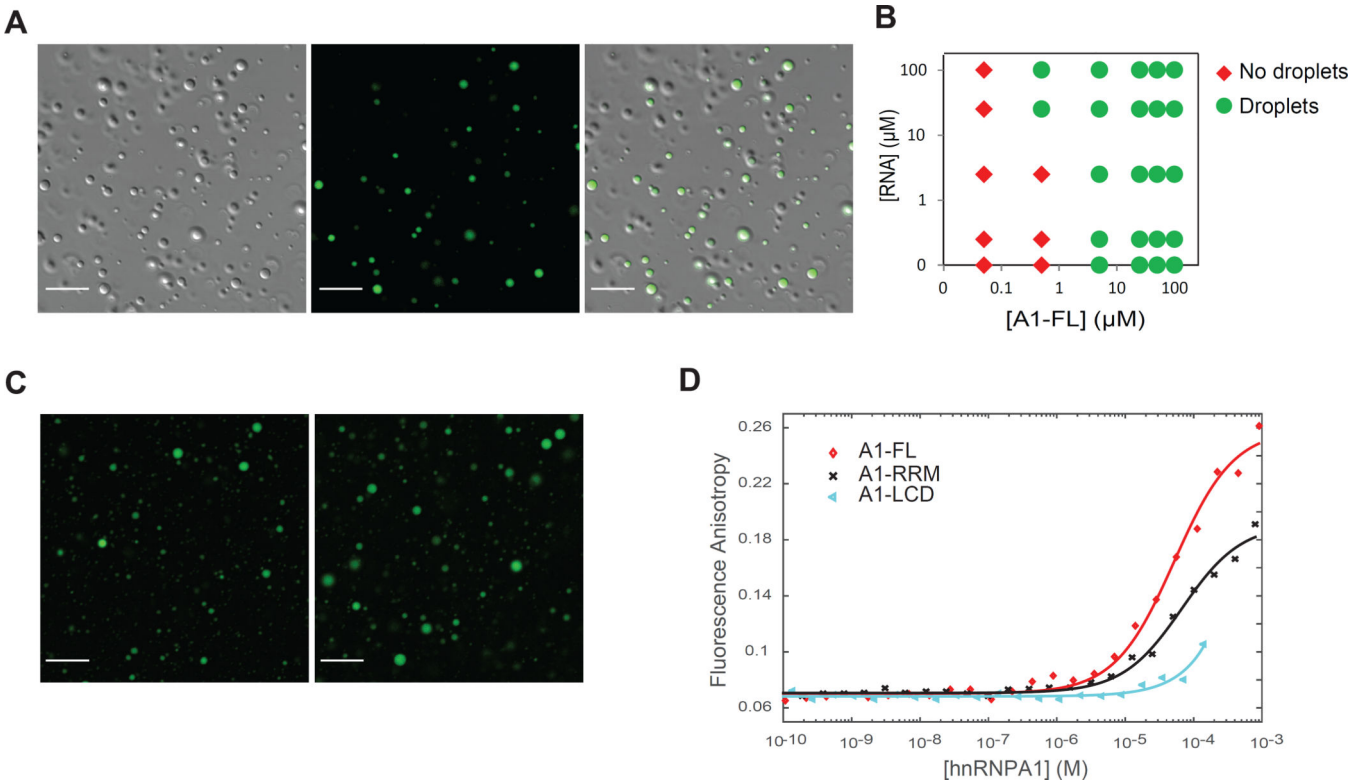

Figure 4. RNA facilitates liquid-liquid phase separation of hnRNPA1 by binding to RRMs and LCD

(A) Fluorescence images of 120 μM hnRNPA1 (DIC) mixed with 1.2 μM fluorescein-labeled RNA at 10 °C. The samples of purified hnRNPA1 were RNA-free (Figure S1).

(B) Phase diagram of hnRNPA1 as a function of protein concentration and RNA concentration. Red and green symbols indicate that the sample was in the one-phase or the two-phase regime, respectively. The experiment was performed in 50 mM HEPES, 150 mM NaCl, 5 mM DTT and 150 mg/ml Ficoll at 10 °C.

(C) Fluorescence images of 100 μM fluorescein-labeled RNA mixed with 100 μM A1-RRM or A1-LCD at 10 °C.

(D) A1-FL, A1-RRM and A1-LCD binding to RNA was monitored by changes in fluorescence anisotropy of 5'-fluorescein-labeled RNA (fl-RNA^{44}). Symbols represent experimental data points, solid lines are non-linear least squares fits to a direct binding model (Roehrl et al., 2004). Importantly, LLPS did not occur under these conditions; the increase in fluorescence anisotropy is therefore caused by direct binding, not partitioning of RNA into droplets.

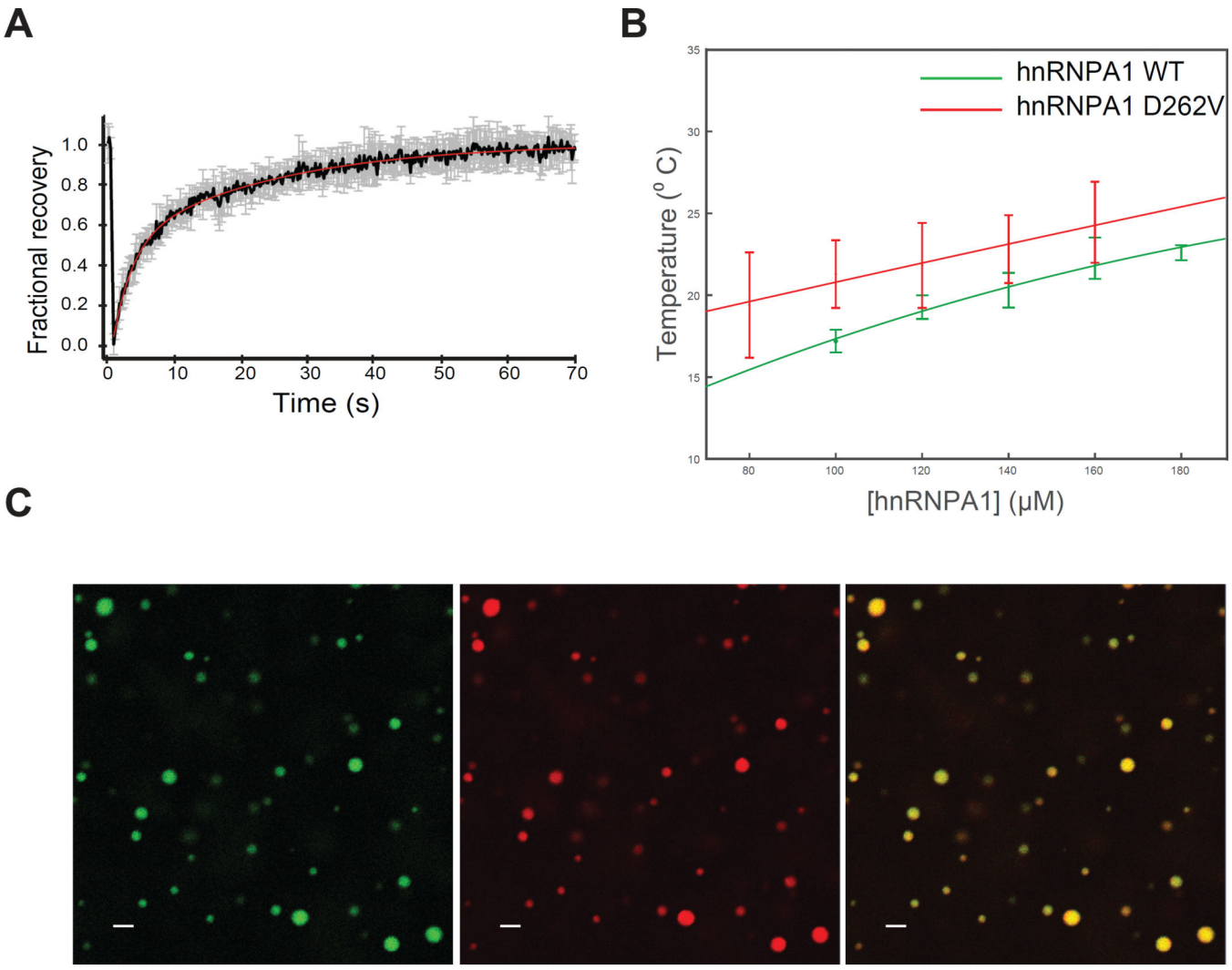

Figure 5. Disease-causing mutant has liquid-liquid phase separation properties similar to the wild-type

(A) FRAP of fluorescently labeled/unlabeled A1 D262V at a molar ratio of 1:300. The black curve is an average of FRAP events from 9 distinct droplets; the error bars represent the standard error. The red curve corresponds to a double exponential fit of the data. The two characteristic recovery times 2.86 s and 23.2 s. See also Table S1.

(B) Phase diagrams of wild-type hnRNPA1 and hnRNPA1-D262V. The apparent cloud point, i.e. the temperature at which droplets were first observed, was determined as a function of protein concentration. Each point represents the mean of a triplicate ± SD. The solid curve represents a fit to a relation for binary demixing from renormalization-group theory. WT data is replotted from Figure 3A.

(C) Fluorescence images of Oregon green-labeled/unlabeled wild-type hnRNPA1 mixed with Rhodamin-Texas red labeled/unlabeled A1-D262V (both at molar ratios of 1:300) at 10 °C.

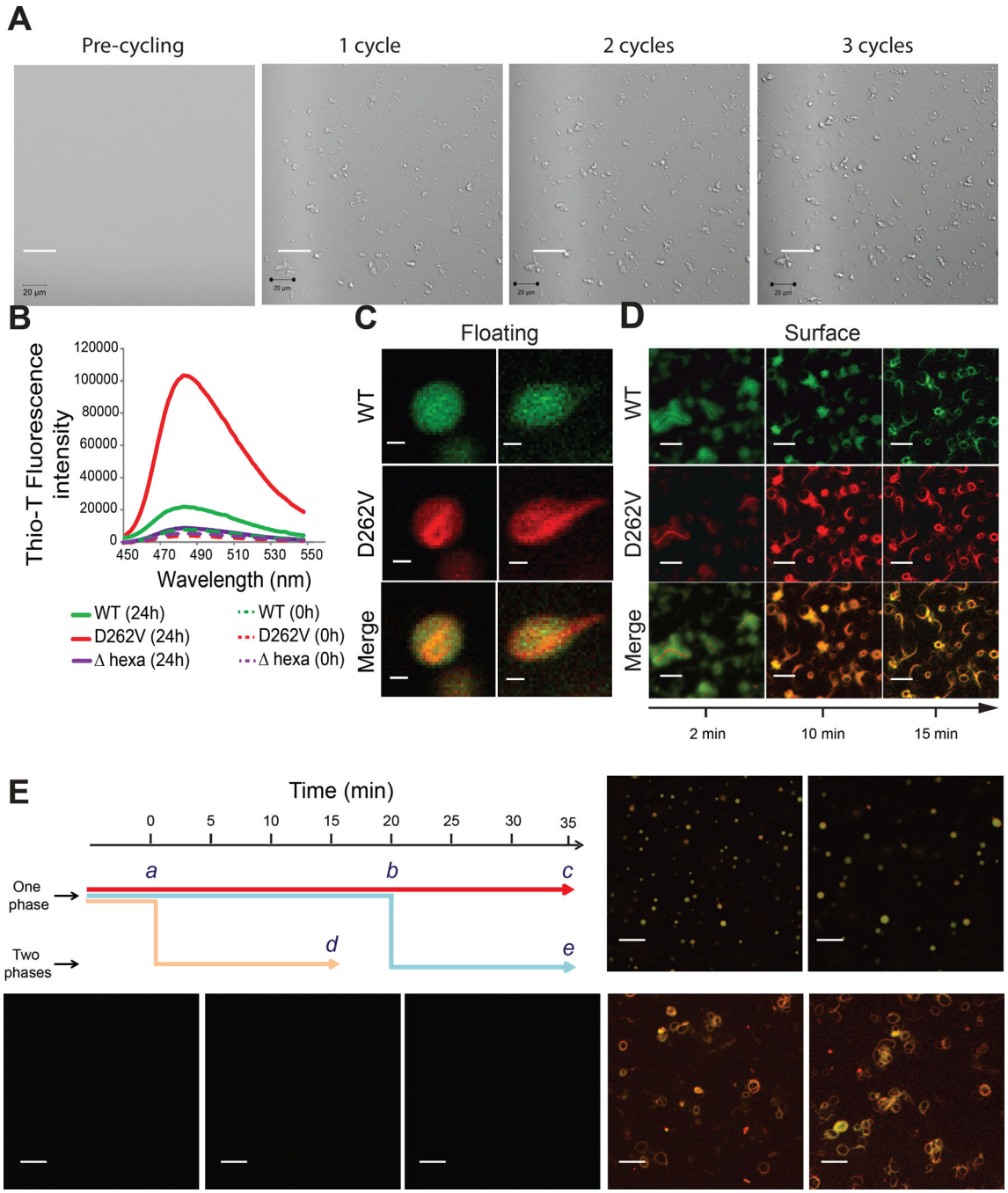

Figure 6. Phase separation promotes fibrillization of hnRNPA1 D262V

All experiments were performed in 50 mM HEPES, 300 mM NaCl, 5 mM DTT and 100 mg/ml Ficoll.

(A) A1-D262V fibrils accumulation on the surface of the coverslip was monitored by cycling the temperature between 10 °C and 25 °C. Each cycle corresponded to a starting temperature of 25 °C, decreased then to 10 °C to allow droplet formation and increased back to 25 °C. The images were taken at 25 °C in order to visualize the surface. See also Figure S6.

(B) A1-FL, A1-D262V or A1-Δhexa were shaken at 25 °C for 24 h. Fibrillization was monitored by ThT fluorescence.

(C) Fluorescence images of floating droplets of a mixture of Oregon green-labeled/unlabeled wild-type hnRNPA1 (total concentration 160 μM, molar ratio of 1:300) mixed with Rhodamin-Texas red labeled/unlabeled A1 D262V (total concentration 160 μM, molar ratio of 1:300) at 16 °C.

(D) Fluorescence images of a mixture of Oregon green-labeled/unlabeled wild-type hnRNPA1 (total concentration 160 μM, molar ratio of 1:300) mixed with Rhodamin-Texas red labeled/unlabeled A1-D262V (total concentration 160 μM, molar ratio of 1:300) at 33 °C. The images were taken at indicated times at the surface of the coverslips.

(E) Schematic summarizing the experiment to correlate phase separation and fibrillization. The sample was either kept in the one-phase regime (33 °C) for 35 min (red arrow), kept in the one-phase regime for 20 min and then put in the two-phase regime by decreasing the temperature to 16 °C for 15 min (blue arrow) or kept in the two-phase regime for 15 min (yellow arrow). The images were taken at the indicated time points (a–e).

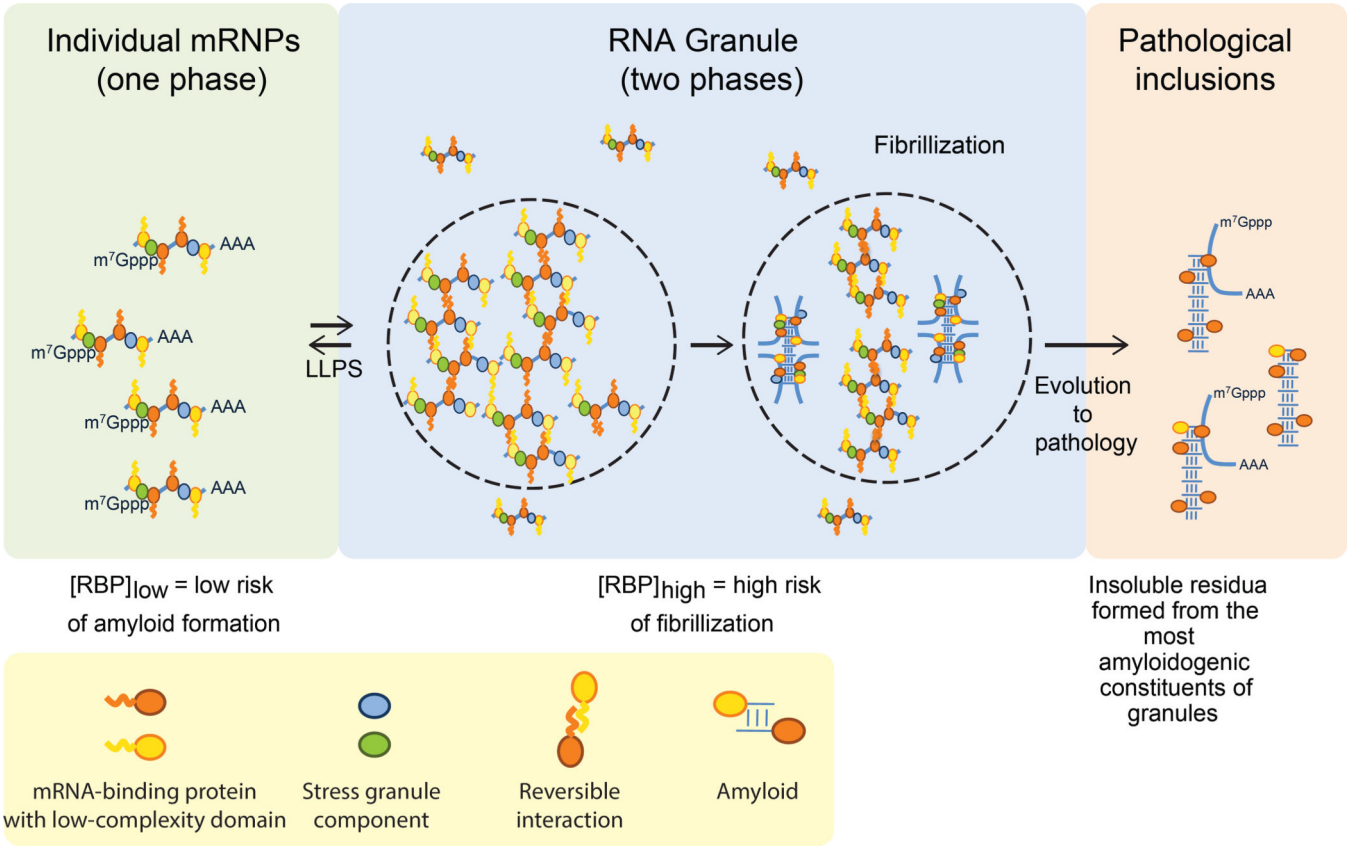

Figure 7. Model

Model depicting the relationship between phase separation, fibrillization and pathological inclusions.